Talanta 202 (2019) 336–341

Contents lists available at ScienceDirect

Talanta

journal homepage: www.elsevier.com/locate/talanta

Label-free Pb^{2+} detection on the layer-by-layer platform using real-time dual polarization interferometry

Shuang Wang[a,b], Shasha Lu[a,b], Jiahui Zhao[a,c], Jianshe Huang[a], Xiurong Yang[a,b,c,*]

[a] State Key Laboratory of Electroanalytical Chemistry, Changchun Institute of Applied Chemistry, Changchun, Jilin, 130022, China
[b] University of Science and Technology of China, Hefei, Anhui, 230026, China
[c] University of Chinese Academy of Sciences, Beijing, 100039, China

ARTICLE INFO

Keywords:
Lead ion
G-quadruplex
Dual polarization interferometry
Biosensor
Layer-by-layer assembly

ABSTRACT

Contamination of Lead ion (Pb^{2+}) poses a serious threat to human health and the environment. Developing sensitive and reliable Pb^{2+} biosensor is essential and significant for prevention and control of the water pollution. In this work, we utilized the direct conformational signal changes in specific interaction process between Pb^{2+} and guanine-rich (G-rich) oligonucleotides to establish a sensing system. The binding of Pb^{2+} and G-rich oligonucleotides results in conformational transition from single strand to G-quadruplex, which was recorded real-time by dual polarization interferometry (DPI). The sensing platform was established via layer-by-layer assembly strategy that employing polyethyleneimine and ploythymine as media layers to link the G-rich DNA on the DPI chip, which is simple, facile and without need of synthesizing sophisticated nanomaterial. On the basis of above sensing platform and quantifiable conformational changes, a simple, sensitive, specific and label-free Pb^{2+} biosensor was established. This research provides us a simple and sensitive method for detection of ions, also encourages us to combine surface technique to biosensing application and explore the relationship between structures and functions.

1. Introduction

Heavy metal pollution has been paid close attention due to its severe harm for human beings' health [1]. As one of typical poisonous heavy metal, lead would damage the central nervous system, cause brain and blood disorders in mammals [2], even destroy the structure of protein and suppress the activity of enzyme via binding with the ligands of biological matters [3]. Therefore, multifarious Pb^{2+} sensors were constructed by virtue of different signal transduction mechanisms, such as fluorescent signal changes resulting from the binding of Pb^{2+} with fluorescent nanomaterials [4,5] or organic molecule [6,7], colorimetric signal changes due to the aggregation function of Pb^{2+} for gold nanoparticle [8–10] or due to the effect of Pb^{2+} on chromogenic reaction [11], electrochemical signal changes caused by the approaching of Pb^{2+} to electrode modified with different functional materials [12–14], and direct detection method such as traditional inductively coupled plasma mass spectrometry (ICP-MS) [15], atomic absorption spectroscopy (AAS) [16]. However, there is a few biosensors were established based on the direct conformational signal changes.

DNA has been attracted considerable attention as a potential material because its predictable structure, specific recognition capability, polymorphism of structure, and biocompatibility, thus is widely employed in biosensing, bioimaging, biocomputing, and drug delivery [17]. Among the various DNA structure, the utilization of G-quadruplex (G4) formed by G-rich sequence takes a great part in biochemical sensing due to its versatile properties. For instance, G4/hemin is a kind of horseradish peroxidase (HRP)-mimicking DNAzyme, could transduces the sensing events through the catalyzed H_2O_2-mediated oxidation of 3,3′,5,5′-tetramethylbenzidine (TMB) [18]/2, 2'-azino-bis(3-ethylbenzothiazoline-6-sulfonic acid) (ABTS) [19]/luminol [20] to blue/chemiluminescent product, generating colorimetric or chemiluminescence readout signals. G4 could also offer binding sites for fluorescent ligand like N-methyl mesoporphyrin IX (NMM) [21], protoporphyrin IX [22] and anthracycline antitumor drugs like doxorubicin and sabarubicin [23,24], giving fluorescent signal output and therapeutic effect. Furthermore, the conformation of G4 could be employed to modulate the distance of donor and acceptor [25], redox probe and electrode surface [26], producing signal changes. Additionally, G4 aptamer could specifically bind with protein like thrombin [27], small molecule like adenosine triphosphate [28], and metal ions like K^+ [29], Sr^{2+} [30], Pb^{2+} [31]. Most of above sensing systems were based on the signal changes resulting from the structural

* Corresponding author. State Key Laboratory of Electroanalytical Chemistry, Changchun Institute of Applied Chemistry, Changchun, Jilin 130022, China.
E-mail address: xryang@ciac.ac.cn (X. Yang).

https://doi.org/10.1016/j.talanta.2019.05.015
Received 21 February 2019; Received in revised form 20 April 2019; Accepted 2 May 2019
Available online 03 May 2019
0039-9140/

changes by introducing or labeling different signal probes, while a few biosensors were constructed based on the direct conformational signal changes.

Dual polarization interferometry (DPI) technique is a well-built and powerful waveguide sensor, which could real-time, label-free monitor the conformational dynamic occurred in the molecule interaction process [32]. Therefore, DPI was widely employed to reveal the connection between function and structure, such as studying the protein crystallization processes [33], the binding process of antibody and antigen [34,35], measuring the membrane perturbation produced by antimicrobial peptides [36,37], characterizing functionalized surface [38,39] and so on. Additionally, the quantitative sensor response function was more sensitive and accurate than classical optical and mass biosensors including surface plasmon resonance, quartz crystal microbalance [40]. Recently, some studies about DNA including its immobilization and hybridization events [41,42], interactions with small molecules were implemented [43–45]. Meanwhile, based on the aforementioned structural changes process of DNA detected by DPI, some biosensors were fabricated. Although DPI-based sensors show excellent sensitivity, specificity, and multiple detection channels, only numbered DPI sensors have been reported.

In this work, a DPI-based Pb^{2+} biosensor is fabricated on the layer-by-layer assembly platform based on the specific interaction of Pb^{2+} and G-rich DNA sequence. G-rich sequences as capture probes were immobilized on the sensing surface. Pb^{2+} could interact with G-rich DNA sequence and form G4, such structural transition would induce the changes of TE and TM phase, the corresponding structural parameters like mass, thickness, density converted from TE and TM were linearly dependent with the concentration of Pb^{2+}. This label-free, simple strategy also exhibits excellent performance in sensitivity, specificity. Meanwhile, the conformational dynamic of G4 could be real-time recorded, which lay the foundation for understanding the physiological process of organism.

2. Materials and methods

2.1. Materials

Poly(ethyleneimine) solution (PEI, MW 750000) was purchased from Sigma-Aldrich (St. Louis, MO). $Pb(Ac)_2{\cdot}3H_2O$, $MgCl_2{\cdot}6H_2O$, $MnCl_2$, and $ZnCl_2$ were provided from Aladdin Chemistry Co. Ltd. (St. Louis, MO). $CaCl_2$, CsCl, KCl were provided from Beijing Chemical Corp. (China). N-(2-hydroxyethyl)-piperazine-N'-ethanesulfonic acid (HEPES) was purchased from Dinguochangsheng Biotechnology Co. (Beijing, China). All reagents were of analytical grade and used as received and without any treatment. DNA oligonucleotides in Table S1 were ordered and synthesized by Sangon Biotechnology Co. Ltd. (Shanghai, China). Before use, the DNA solutions needed to be heated at 95 °C for 5 min and then slowly cooled down to room temperature. Milli-Q water system was used to prepare ultrapure water of 18.25 MΩ cm. The lake water were got from local South Lake in Changchun. 25 mM HEPES buffer (100 mM NaAc, pH 7.4) and lake water were used after filtering and degassing.

2.2. Circular dichroism (CD) and UV–vis absorption spectra experiments

200 μL of mixed solution containing 5 μM capture probe (or control probe) and 10 μM Pb^{2+} ions reacted for 40 min at room temperature, then were measured on a Jasco J-820 circular dichroism spectra polarimeter (Tokyo, Japan). 100 μL of mixed solution containing 1 μM capture probe (or control probe) and 10 μM Pb^{2+} ions reacted for 40 min at room temperature, then were measured on a CARY 500 UV–vis–NIR Varian spectrophotometer. The ultimate reported circular dichroism (CD) and UV–vis absorption spectra were the average of three parallel data. In order to explicitly compare the conformational changes between the capture probe and control probe, we plotted their CD and UV–vis differential spectra. The CD and UV–vis spectra of capture probe/control probe in presence of Pb^{2+} were subtracted from that in absence of Pb^{2+} to obtain the respective differential spectra.

2.3. DPI experiments

The establishment of sensing platform and the specific binding process of G-rich DNA sequence and Pb^{2+} were monitored in real-time by utilizing a DPI instrument (AnaLight Bio200, Farfield). In the whole DPI experimental process, 25 mM HEPES solution as running buffer flowed the channels. First, the unmodified silicon oxynitride chip was installed on the instrument, and the flow rate of running buffer was set at 100 μL/min to remove the air in the channels quickly and keep the baseline stable. Second, the chip and running buffer calibrations were executed using 80% (v/v) ethanol/water solution and ultrapure water with known refractive indexes. Third, the construction of sensing platform was explained in more detail as follows: 0.1 mg/mL polyetherimide (PEI) was applied to both channels at 50 μL/min for 4 min, then the running buffer returned to both channel until the baseline reached stable. Subsequently, 8 μM T30 was introduced for 4 min at 50 μL/min and then incubated for 10 min. When the baseline was stable again, 8 μM A15-AS1411 was introduced into the channel to hybridize with T30. Finally, Pb^{2+} with different concentrations flowed over the channel for 4 min and reacted with the A15-AS1411 for another 5 min, respectively. Until all the samples were injected and the baseline reached stable, we stopped the experiment. The thickness, refractive index, density, and mass values were acquired with the AnaLight DAQ software, which used in the further construction of Pb^{2+} biosensor.

2.4. Pb^{2+} detection in lake water

To verify the practicability of our biosensing method, we detected Pb^{2+} in lake water. We fabricated the same biosensing surface according to aforementioned procedure of construction of sensing platform. Then we quantified the spiked Pb^{2+} with different concentrations in 1% lake water using DPI technique and compared above detection result with that obtained by ICP-AES method.

3. Results and discussion

3.1. Construction of biosensing platform for Pb^{2+} detection

There are two indispensable elements in the construction of biosensing platform, which are the choice for capture probe and the connection method of capture probe on sensing chip, respectively. First, we choose a DNA probe AS1411 as the capture probe for Pb^{2+}, because it was reported that AS1411 could bind with Pb^{2+} strongly and specifically, forming typical G4 structure [46,47]. Furthermore, AS1411 is a quadruplex-forming oligonucleotide aptamer that targets nucleolin, its biological effect was embodied in inhibiting cancer cell proliferation. Therefore, the establishment of our sensing platform could not only detect hazardous Pb^{2+}, but also would lay the foundation of understanding the pathogenesis and designing disease-fighting drugs. Second, we choose a simple and explicit method to immobilize the DNA probe on the sensing surfaces. As displayed in Scheme 1, the polycation complex (polyethyleneimine, PEI) was firstly immobilized on the unmodified silicon oxynitride chip, which could act a linker between chip and negatively charged ploythymine (T30) via electrostatic adsorption. T30 had two functions: connect A15-AS1411 on the sensing surface and increase the distance between PEI and A15-AS1411, which could effectively overcome the strong electrostatic resistance from PEI and improve the flexibility of capture probe. After the successful construction of sensing surfaces, Pb^{2+} with different concentrations were introduced into the sensing surfaces, AS1411 at one end of capture probe will capture Pb^{2+}, showing conformational transition from random single strand to G4. The direct conformational change signals were

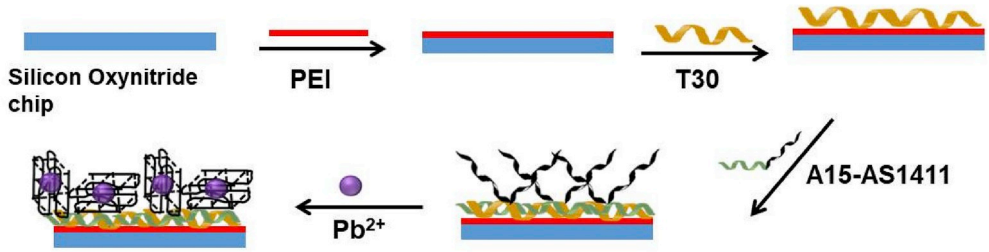

Scheme 1. Schematic illustration of the construction of sensing surface and Pb^{2+} detection process.

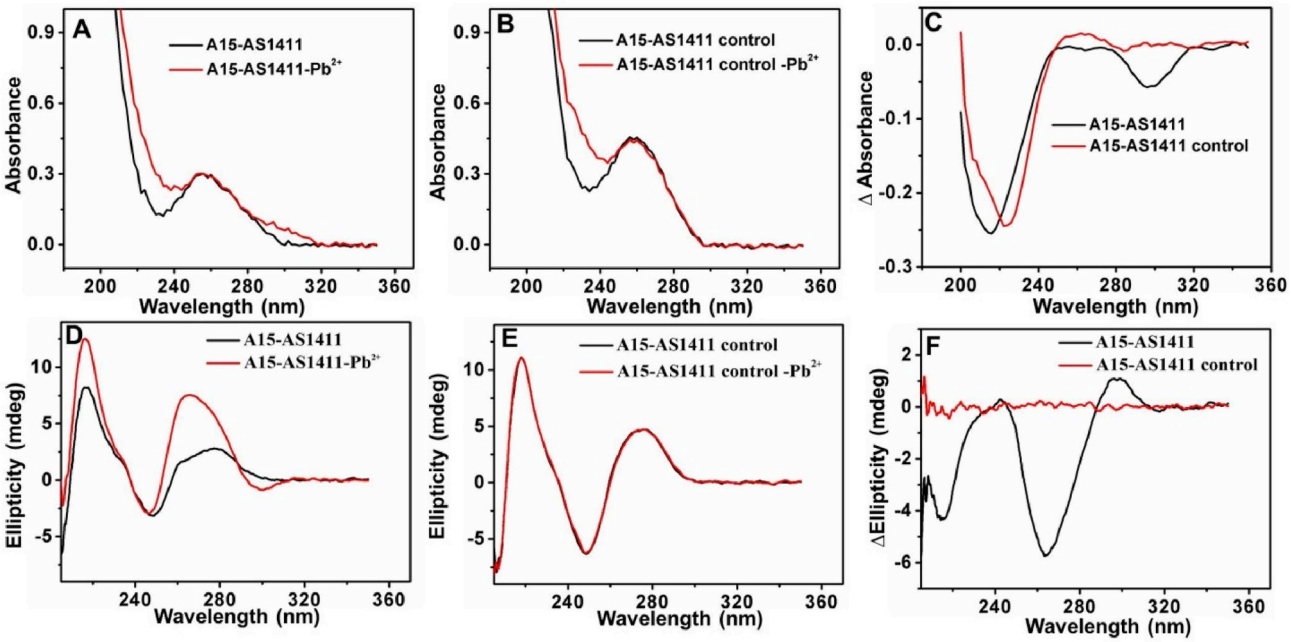

Fig. 1. UV–vis spectra of A15-AS1411 (A), A15-AS1411 control (B) in presence and absence of Pb^{2+} and their differential spectrometry. CD spectra of A15-AS1411 (D), A15-AS1411 control (E) in presence and absence of Pb^{2+} and their differential spectrometry.

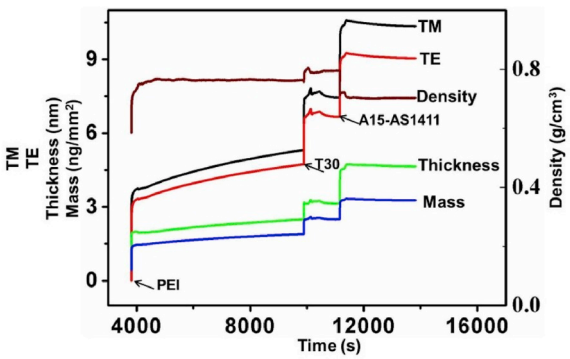

Fig. 2. TM (black line), TE (red line), density (wine red line), thickness (green line) and mass (blue line) changes occurred in the whole process of constructing sensing interface. (For interpretation of the references to color in this figure legend, the reader is referred to the Web version of this article.)

employed to quantify the Pb^{2+} in the system.

3.2. UV–vis and circular dichroism (CD) spectra characterization of interaction of Pb^{2+} and G-rich DNA sequences

Before executing the DPI sensing function, we should assure that the capture probe actually could interact with Pb^{2+} and the process was accompanied by conformational changes. As displayed in Fig. 1, the absorbance of A15-AS1411 has an increase around 300 nm upon adding Pb^{2+}, while the A15-AS1411 control strand has negligible changes. Above hyperchroism peak around 300 nm attributes to the specific guanine – guanine stacking [48], which manifests the formation of G4. In order to distinguish the absorbance difference at 300 nm, the UV–vis differential spectrometry of A15-AS1411 and its control strand were plotted in Fig. 1C. The CD spectra of A15-AS1411 in Fig. 1D and E demonstrates that typical positive peaks at 220 and 265 nm increase upon adding Pb^{2+}, representing formation of parallel G4 structure [49], while the CD spectra of A15-AS1411 control strand have no changes before and after adding Pb^{2+}. The CD differential spectrometry of capture DNA has an obvious conformational transition, while that of the control DNA closes to a straight line which suggests unchanged conformation (Fig. 1F). Above results verify that the A15-AS1411 has the ability to bind with Pb^{2+} and shows a structural transition from single strand to G4, which also preliminarily proves our proposed strategy is feasible.

3.3. Construction of sensing surface monitored by DPI

Under the premise of ensuring feasibility, we carried out the monitoring for the construction of sensing surface by DPI. As shown in Fig. 2, when different samples including PEI, T30, and A15-AS1411 were injected on the sensing chip, TM (black line) and TE (red line) phase have corresponding changes. Based on the TM and TE changes, the conformational parameters like density, mass and thickness were analyzed out, which was benefit for the understanding for the interaction process. For example, as the PEI was flowed over the chip, the

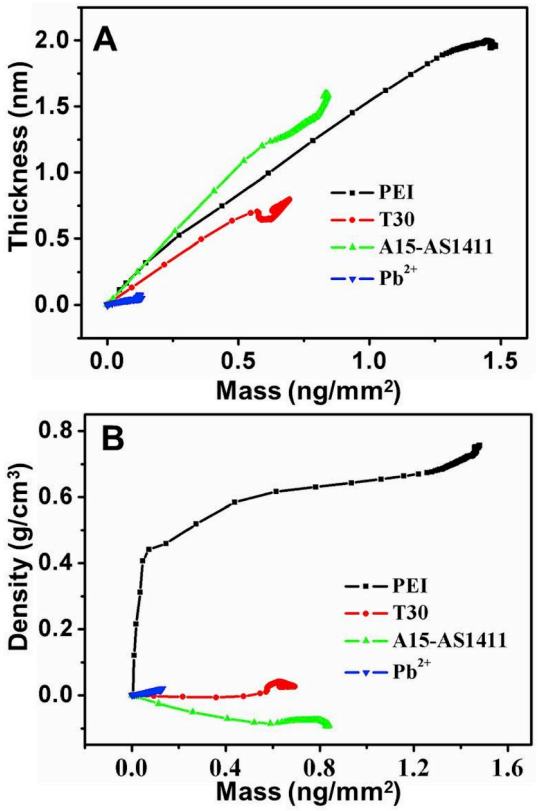

Fig. 3. Conformational dynamic of the whole construction process of biosensing surfaces. Plot thickness (A) and density (B) as a function of mass per area. The concentration of PEI, T30, A15-AS1411, and Pb^{2+} were 0.1 mg/mL, 8 μM, 8 μM and 100 μM, respectively.

thickness, mass and density had a rapid increase; subsequently, the increased rate slowed down, which meant the absorption of PEI tended to saturation. Gradually the density had slight drop while the thickness and mass still increased, which ascribed to swelling property of PEI [50]. When T30 was absorbed on the PEI layer, the thickness and mass increased evidently, and the density had an unobvious increase, which disagreed with previous report [51]. We speculated this was because the PEI at high concentration enabled T30 attach on the surface tightly instead of depositing on the chip sparsely. As the number of DNA layer increased, the upper A15-AS1411 would be less affected by PEI. Therefore, the thickness and mass increased, density decreased obviously when A15-AS1411 was introduced, which was consistent with previous report [40,51].

In order to clear the conformational dynamic in the whole process, we plotted the thickness (Fig. 3A) and density (Fig. 3B) of mass. Due to the same collecting frequency of data, we could clear the absorption rate easily according to the distribution of the data points. For instance, the sparse data dots at the beginning of injecting suggested the quick absorption, and the dense dots meant that the interaction establishes equilibrium continuously. At the end of injecting, the thickness and density have slight changes, inferring the conformation was rearranged to a stable state. As observed in Fig. 3A, the thickness increased as the mass increased when PEI, T30, A15-AS1411, Pb^{2+} were introduced into the channel. From the thickness, we could know their spatial distribution. On the basis of the density changes as the increased mass, we could roughly estimate the surface state. For example, T30 had no obvious increase in density, which implied that T30 could attached on PEI in a relatively compact state; while there is apparent decrease when A15-AS1411 was injected, which hinted that A15-AS1411 did not insert in the T30/PEI layer rather than deposit on it in a relatively loose state. Combining thickness with density changes as the mass, we could further infer their interaction modes.

3.4. Performance of proposed DPI-based Pb^{2+} biosensor

On the basis of our proposed biosensing mechanism, we implemented quantitative detection of Pb^{2+} using DPI. As shown in Fig. 4, the mass, thickness and density increased as Pb^{2+} concentration increased, and these three DPI signals were linearly dependent on the Pb^{2+} concentration. The respective detection limits were 2.8 nM, 3.58 nM, 6.96 nM based on mass, thickness and density calibration, which are comparable to, even better than some reported Pb^{2+} sensors

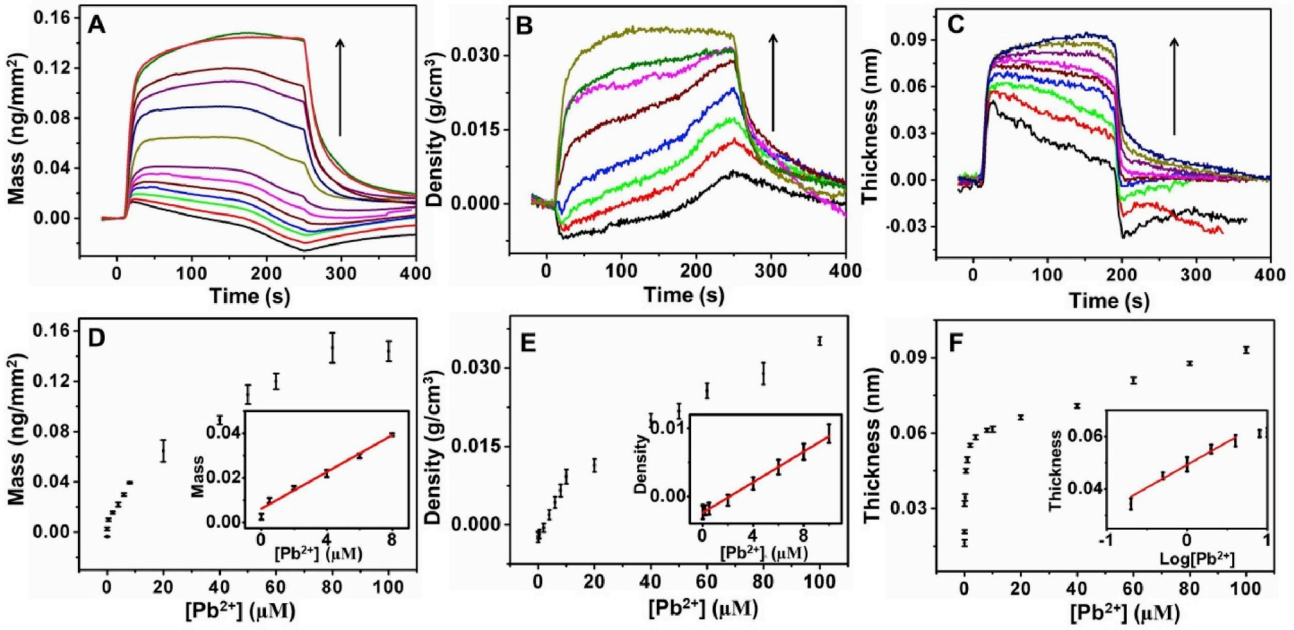

Fig. 4. Linearity of our designed biosensor. Mass (A), density (B) and thickness (C) changes of the proposed Pb^{2+} biosensor with increasing concentration ranging 0–100 μM. The concentration of PEI, T30, and A15-AS1411 were 0.1 mg/mL, 8 μM, and 8 μM, respectively. The error bars represent the standard deviation of three measurements.

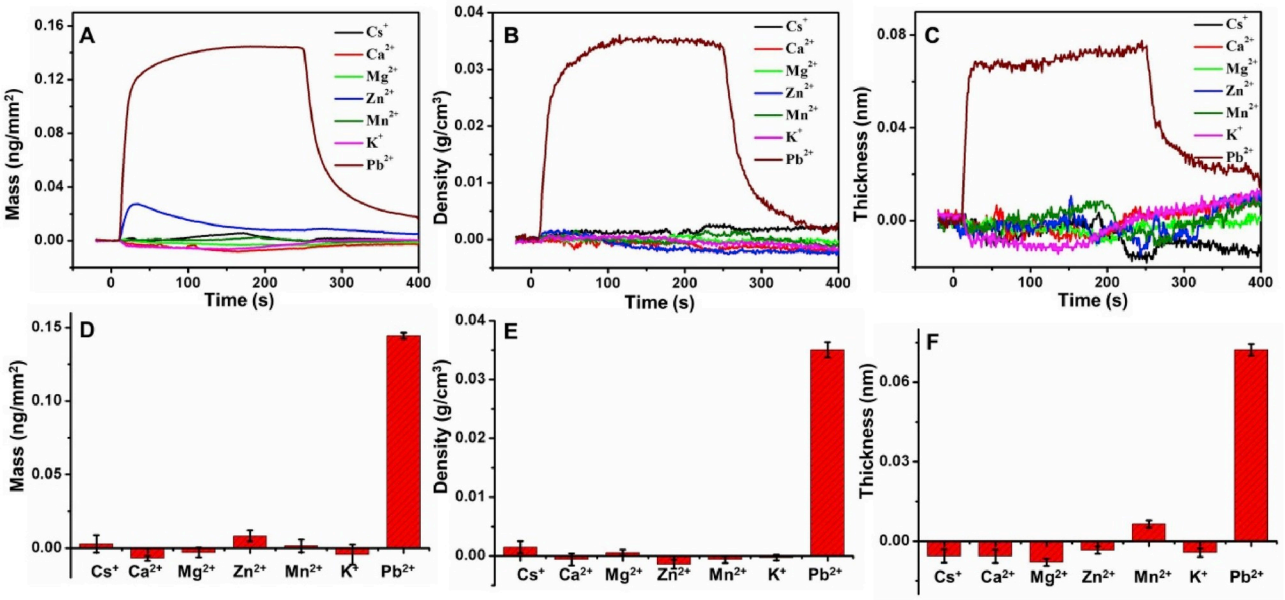

Fig. 5. Selectivity of the proposed Pb^{2+} biosensor. Comparing the mass, density and thickness changes induced by Pb^{2+} with control metal ions including Cs^{+}, Ca^{2+}, Na^{+}, Mg^{2+}, Zn^{2+}, Mn^{2+}, and K^{+}. The concentration of all samples was 100 μM. The error bars were obtained based on three measurements.

[3,12,52–54]. Also these results are much lower than the lowest limit of Pb^{2+} (0.24 μM) in drinking water regulated by World Health Organization, suggesting our proposed biosensor could be used for monitoring water pollution.

3.5. Specificity and selectivity of DPI-based Pb^{2+} biosensor

To evaluate the selectivity of the fabricated biosensor, we compared the conformational changes induced by different metal ions including Pb^{2+}, Zn^{2+}, Na^{+}, Mn^{2+}, Mg^{2+}, Ca^{2+}, Cs^{+}, and K^{+}. Only Pb^{2+} could bind with capture probe (increased distinctly mass) and have obvious conformational changes (increased distinctly density and thickness), while other control metal ions had less obvious response (Fig. 5). Additionally, we replaced the capture probe with control probe which cannot specifically bind with Pb^{2+}. Compared with the increased continuously density, thickness, and mass as the increased Pb^{2+}, the control probe had less change than capture probe (Fig. S1). Above results prove that our fabricated Pb^{2+} biosensor possesses excellent specificity and selectivity.

3.6. Pb^{2+} detection in real sample

In order to investigate the practical value of our sensing method, we tested Pb^{2+} in lake water. The comparison among spiked concentration, real concentration detected by mass calibration of DPI and real concentration detected by ICP-AES method was shown in Fig. S2, the close result demonstrates that our detection strategy is credible and has potential for further detection in real sample.

4. Conclusions

In summary, label-free and real-time DPI technique was used to investigate the interaction between Pb^{2+} and G-rich DNA sequence on the layer-by-layer assembled biosensing platform. DPI could not only supply real-time structural information, but also quantify the conformation changes, giving a sensor response function. Pb^{2+} could specifically interacted with G-rich DNA sequences, accompanying by the formation of G4. While the control metal ions and control strand showed no distinct changes, which were in accord with CD and UV–vis spectra results. On the basis of above property, a simple, sensitive, specific, label-free and real-time DPI-based Pb^{2+} biosensor was established successfully. Such DPI-based Pb^{2+} biosensor on layer-by-layer assembly platform has several merits: first, the biosensing mechanism is well-known, simple and clear; second, the preparation of layer-by-layer assembled biosensing platform is simple, facile, and without the need of synthesizing complicated nanomaterials and designing intricate DNA primer; third, DPI-based sensing platform actually has two sensor channels, which could realize the multiplex detection function. Our attempt for the monitoring of G-rich sequence behavior not only encourages researchers to explore the interaction of DNA with other molecules, but also inspires us to further discover the unbeknown physiological processes in body by DPI technique.

Declarations of interest

None.

Acknowledgment

This work was supported by the National Natural Science Foundation of China [No. 21627808, 21435005]; Key Research Program of Frontier Sciences, CAS [QYZDY-SSW-SLH019]; and the Development Project of Science and Technology of Jilin Province [No. 20170101195JC].

Appendix A. Supplementary data

Supplementary data to this article can be found online at https://doi.org/10.1016/j.talanta.2019.05.015.

References

[1] T. Li, E. Wang, S. Dong, Lead(II)-Induced allosteric G-quadruplex DNAzyme as a colorimetric and chemiluminescence sensor for highly sensitive and selective Pb2+ detection, Anal. Chem. 82 (2010) 1515–1520.
[2] H.N. Kim, W.X. Ren, J.S. Kim, J. Yoon, Fluorescent and colorimetric sensors for detection of lead, cadmium, and mercury ions, Chem. Soc. Rev. 41 (2012) 3210–3244.
[3] G. Zhou, J. Chang, S. Cui, H. Pu, Z. Wen, J. Chen, Real-time, selective detection of Pb2+ in water using a reduced graphene oxide/gold nanoparticle field-effect transistor device, ACS Appl. Mater. Interfaces 6 (2014) 19235–19241.
[4] H. Kawasaki, K. Hamaguchi, I. Osaka, R. Arakawa, Ph-dependent synthesis of pepsin-mediated gold nanoclusters with blue green and red fluorescent emission,

Adv. Funct. Mater. 21 (2011) 3508–3515.
[5] E. Mohamed Ali, Y. Zheng, H.-h. Yu, J.Y. Ying, Ultrasensitive Pb2+ detection by glutathione-capped quantum dots, Anal. Chem. 79 (2007) 9452–9458.
[6] S.K. Kim, S.H. Lee, J.Y. Lee, J.Y. Lee, R.A. Bartsch, J.S. Kim, An excimer-based, binuclear, on-off switchable calix 4 crown chemosensor, J. Am. Chem. Soc. 126 (2004) 16499–16506.
[7] J.Y. Kwon, Y.J. Jang, Y.J. Lee, K.M. Kim, M.S. Seo, W. Nam, J. Yoon, A highly selective fluorescent chemosensor for Pb2+, J. Am. Chem. Soc. 127 (2005) 10107–10111.
[8] F. Chai, C.A. Wang, T.T. Wang, L. Li, Z.M. Su, Colorimetric detection of Pb2+ using glutathione functionalized gold nanoparticles, ACS Appl. Mater. Interfaces 2 (2010) 1466–1470.
[9] J.W. Liu, Y. Lu, Accelerated color change of gold nanoparticles assembled by DNAzymes for simple and fast colorimetric Pb2+ detection, J. Am. Chem. Soc. 126 (2004) 12298–12305.
[10] D.B. Liu, Z. Wang, X.Y. Jiang, Gold nanoparticles for the colorimetric and fluorescent detection of ions and small organic molecules, Nanoscale 3 (2011) 1421–1433.
[11] H. Liu, Y. Ji, C. Song, G. Tian, S. Li, G. Yang, C. Lyu, Pb～(2+)-Induced allosteric PS2.M as A label-free colorimetric sensor for detection of cumulative radon radiation, Chin. J. Anal. Chem. 46 (2018) 658–663.
[12] F. Cai, Q. Wang, X. Chen, W. Qiu, F. Zhan, F. Gao, Q. Wang, Selective binding of Pb2+ with manganese-terephthalic acid MOF/SWCNTs: Theoretical modeling, experimental study and electroanalytical application, Biosens. Bioelectron. 98 (2017) 310–316.
[13] L. Shen, Z. Chen, Y.H. Li, S.L. He, S.B. Xie, X.D. Xu, Z.W. Liang, X. Meng, Q. Li, Z.W. Zhu, M.X. Li, X.C. Le, Y.H. Shao, Electrochemical DNAzyme sensor for lead based on amplification of DNA-Au bio-bar codes, Anal. Chem. 80 (2008) 6323–6328.
[14] C.-Y. Gao, J.-H. Tong, C. Bian, J.-Z. Sun, Y. Li, J.-F. Wang, S. Gong, Y. Hui, Y.-H. Xu, X.-Q. Wang, H.-C. Xie, S.-H. Xia, Determination of trace Zn(II), Cd(II) and Pb(II) metal ions using in-situ bismuth-modified boron doped diamond electrode, Chin. J. Anal. Chem. 46 (2018) 217–224.
[15] M. Corte Rodríguez, R. Álvarez-Fernández García, E. Blanco, J. Bettmer, M. Montes-Bayón, Quantitative evaluation of cisplatin uptake in sensitive and resistant individual cells by single-cell ICP-MS (SC-ICP-MS), Anal. Chem. 89 (2017) 11491–11497.
[16] M. Ghaedi, F. Ahmadi, A. Shokrollahi, Simultaneous preconcentration and determination of copper, nickel, cobalt and lead ions content by flame atomic absorption spectrometry, J. Hazard Mater. 142 (2007) 272–278.
[17] S. Wang, J. Sun, J. Zhao, S. Lu, X. Yang, Photo-induced electron transfer-based versatile platform with G-quadruplex/hemin complex as quencher for construction of DNA logic circuits, Anal. Chem. 90 (2018) 3437–3442.
[18] B.-C. Yin, B.-C. Ye, W. Tan, H. Wang, C.-C. Xie, An allosteric dual-DNAzyme unimolecular probe for colorimetric detection of copper(II), J. Am. Chem. Soc. 131 (2009) 14624–14625.
[19] D. Li, B. Shlyahovsky, J. Elbaz, I. Willner, Amplified analysis of low-molecular-weight substrates or proteins by the self-assembly of DNAzyme－Aptamer conjugates, J. Am. Chem. Soc. 129 (2007) 5804–5805.
[20] R. Freeman, X. Liu, I. Willner, Chemiluminescent and chemiluminescence resonance energy transfer (CRET) detection of DNA, metal ions, and aptamer–substrate complexes using hemin/G-quadruplexes and CdSe/ZnS quantum dots, J. Am. Chem. Soc. 133 (2011) 11597–11604.
[21] J.M. Nicoludis, S.P. Barrett, J.-L. Mergny, L.A. Yatsunyk, Interaction of human telomeric DNA with N-methyl mesoporphyrin IX, Nucleic Acids Res. 40 (2012) 5432–5447.
[22] J. Zhu, L. Zhang, S. Dong, E. Wang, Four-way junction-driven DNA strand displacement and its application in building majority logic circuit, ACS Nano 7 (2013) 10211–10217.
[23] I. Manet, F. Manoli, B. Zambelli, G. Andreano, A. Masi, L. Cellai, S. Monti, Affinity of the anthracycline antitumor drugs Doxorubicin and Sabarubicin for human telomeric G-quadruplex structures, Phys. Chem. Chem. Phys. 13 (2011) 540–551.
[24] J.-L. Mergny, L. Lacroix, M.-P. Teulade-Fichou, C. Hounsou, L. Guittat, M. Hoarau, P.B. Arimondo, J.-P. Vigneron, J.-M. Lehn, J.-F. Riou, T. Garestier, C. Hélène, Telomerase inhibitors based on quadruplex ligands selected by a fluorescence assay, Proc. Natl. Acad. Sci. Unit. States Am. 98 (2001) 3062–3067.
[25] K.S. Park, M.W. Seo, C. Jung, J.Y. Lee, H.G. Park, Simple and universal platform for logic gate operations based on molecular beacon probes, Small 8 (2012) 2203–2212.
[26] A.-E. Radi, J.L. Acero Sánchez, E. Baldrich, C.K. O'Sullivan, Reagentless, reusable, ultrasensitive electrochemical molecular beacon aptasensor, J. Am. Chem. Soc. 128 (2006) 117–124.
[27] C.W. Liu, C.C. Huang, H.T. Chang, Highly selective DNA-based sensor for lead(II) and mercury(II) ions, Anal. Chem. 81 (2009) 2383–2387.
[28] N. Lu, C. Shao, Z. Deng, Rational design of an optical adenosine sensor by conjugating a DNA aptamer with split DNAzyme halves, Chem. Commun. 46 (2008) 6161–6163.
[29] D.-M. Kong, J.-H. Guo, W. Yang, Y.-E. Ma, H.-X. Shen, Crystal violet–G-quadruplex complexes as fluorescent sensors for homogeneous detection of potassium ion, Biosens. Bioelectron. 25 (2009) 88–93.
[30] E. Largy, A. Marchand, S. Amrane, V. Gabelica, J.-L. Mergny, Quadruplex turncoats: cation-dependent folding and stability of quadruplex-DNA double switches, J. Am. Chem. Soc. 138 (2016) 2780–2792.
[31] F. Li, Y. Feng, C. Zhao, B. Tang, Crystal violet as a G-quadruplex-selective probe for sensitive amperometric sensing of lead, Chem. Commun. 47 (2011) 11909–11911.
[32] J. Escorihuela, M.A. Gonzalez-Martinez, J.L. Lopez-Paz, R. Puchades, A. Maquieira, D. Gimenez-Romero, Dual-polarization interferometry: a novel technique to light up the nanomolecular world, Chem. Rev. 115 (2015) 265–294.
[33] A. Boudjemline, E. Saridakis, M.J. Swann, L. Govada, I.M. Mavridis, N.E. Chayen, Use of dual polarization interferometry as a diagnostic tool for protein crystallization, Anal. Chem. 83 (2011) 7881–7887.
[34] B.J. Cowsill, T.A. Waigh, S. Eapen, R. Davies, J.R. Lu, Interfacial structure and history dependent activity of immobilised antibodies in model pregnancy tests, Soft Matter 8 (2012) 9847–9854.
[35] D. Giménez-Romero, M.A. González-Martíne, M.-J. Bañuls, I.S. Monzó, R. Puchades, Á. Maquieira, Modeling of the role of conformational dynamics in kinetics of the antigen–antibody interaction in heterogeneous phase, J. Phys. Chem. B 116 (2012) 5679–5688.
[36] J. Popplewell, N. Freeman, S. Carrington, G. Ronan, C. McDonnell, R.C. Ford, Quantification of the effects of melittin on liposome structure, Biochem. Soc. Trans. 33 (2005) 931–933.
[37] L. Tzong-Hsien, N.H. Kristopher, A. Marie-Isabel, Antimicrobial peptide structure and mechanism of action: a focus on the role of membrane structure, Curr. Top. Med. Chem. 16 (2016) 25–39.
[38] M. Duan, H. Wang, S. Fang, Y. Liang, Real-time monitoring the adsorption of sodium dodecyl sulfate on a hydrophobic surface using dual polarization interferometry, J. Colloid Interface Sci. 417 (2014) 285–292.
[39] C.F. Carlborg, K.B. Gylfason, A. Kazmierczak, F. Dortu, M.J. Banuls Polo, A. Maquieira Catala, G.M. Kresbach, H. Sohlstrom, T. Moh, L. Vivien, J. Popplewell, G. Ronan, C.A. Barrios, G. Stemme, W. van der Wijngaart, A packaged optical slot-waveguide ring resonator sensor array for multiplex label-free assays in labs-on-chips, Lab Chip 10 (2010) 281–290.
[40] S. Wang, S. Lu, J. Zhao, J. Huang, X. Yang, Real-time study of the interaction between G-rich DNA oligonucleotides and lead ion on DNA tetrahedron-functionalized sensing platform by dual polarization interferometry, ACS Appl. Mater. Interfaces 9 (2017) 41568–41576.
[41] P. Xu, F. Huang, H. Liang, Real-time study of a DNA strand displacement reaction using dual polarization interferometry, Biosens. Bioelectron. 41 (2013) 505–510.
[42] F. Huang, P. Xu, H. Liang, Using dual-polarization interferometry to study surface-initiated DNA hybridization chain reactions in real time, Biosens. Bioelectron. 51 (2014) 317–323.
[43] Y. Zheng, C. Yang, F. Yang, X. Yang, Real-time study of interactions between cytosine–cytosine pairs in DNA oligonucleotides and silver ions using dual polarization interferometry, Anal. Chem. 86 (2014) 3849–3855.
[44] Y. Zheng, T. Hu, C. Chen, F. Yang, X. Yang, An anti-fouling aptasensor for detection of thrombin by dual polarization interferometry, Chem. Commun. 51 (2015) 5645–5648.
[45] T. Hu, F. Yang, X.-R. Yang, Real-time study of interaction between adenosine triphosphate and its aptamer using dual polarization interferometry, Chin. J. Anal. Chem. 45 (2017) 944–950.
[46] Z. Bagheri, B. Ranjbar, H. Latifi, M.I. Zibaii, T.T. Moghadam, A. Azizi, Spectral properties and thermal stability of AS1411 G-quadruplex, Int. J. Biol. Macromol. 72 (2015) 806–811.
[47] Y. Teng, A.C. Girvan, L.K. Casson, W.M. Pierce, M. Qian, S.D. Thomas, P.J. Bates, AS1411 alters the localization of a complex containing protein arginine methyltransferase 5 and nucleolin, Cancer Res. 67 (2007) 10491–10500.
[48] K.A. Ioannis, H.N. Ma'ani, N. Ettore, S.G. Piero, R. Antonio, W.d.S. Mateus, Topological characterization of nucleic acid G-quadruplexes by UV absorption and circular dichroism, Angew. Chem. Int. Ed. 50 (2011) 10645–10648.
[49] J. Kypr, I. Kejnovská, D. Renčiuk, M. Vorlíčková, Circular dichroism and conformational polymorphism of DNA, Nucleic Acids Res. 37 (2009) 1713–1725.
[50] Y. Wang, Y. Zheng, F. Yang, X. Yang, Dual polarisation interferometry for real-time, label-free detection of interaction of mercury(II) with mercury-specific oligonucleotides, Chem. Commun. 48 (2012) 2873–2875.
[51] Y. Zheng, C. Yang, F. Yang, X. Yang, Real-time study of interactions between Cytosine－Cytosine pairs in DNA oligonucleotides and silver ions using dual polarization interferometry, Anal. Chem. 86 (2014) 3849–3855.
[52] X. Liu, Y. Wang, Y. Song, Visually multiplexed quantitation of heavy metal ions in water using volumetric bar-chart chip, Biosens. Bioelectron. 117 (2018) 644–650.
[53] D.G. Khandare, H. Joshi, M. Banerjee, M.S. Majik, A. Chatterjee, An aggregation-induced emission based "turn-on" fluorescent chemodosimeter for the selective detection of Pb2+ ions, RSC Adv. 4 (2014) 47076–47080.
[54] J.-M. Jian, Y.-Y. Liu, Y.-L. Zhang, X.-S. Guo, Q. Cai, Fast and sensitive detection of Pb2+ in foods using disposable screen-printed electrode modified by reduced graphene oxide, Sensors 13 (2013) 13063–13075.